

# Blueshifted [O III] Emission: Indications of a Dynamic NLR

Todd Boroson

*National Optical Astronomy Observatories, Tucson, AZ 85719*

tyb@noao.edu

## ABSTRACT

The [O III]  $\lambda 5007$  line is commonly used as an indicator of the systemic redshift of AGNs. Also, recent studies have used the width of this emission line as a proxy for the stellar velocity dispersion in the host galaxy. This paper calls both of these assumptions into question by analyzing a sample of approximately 400 AGN spectra from the first data release of the Sloan Digital Sky Survey. These spectra show that the low-ionization forbidden lines ([O II], [N II], [S II]) define a consistent redshift, but that the peak of the [O III] line is blueshifted in approximately half of the AGNs with respect to that redshift. For the sample studied here, the average shift is  $40 \text{ km s}^{-1}$ , with the largest shift being over  $400 \text{ km s}^{-1}$ . The magnitude of this shift is found to be correlated with a number of properties, including the width of the [O III] line and the Eddington ratio ( $L/L_{\text{Edd}}$ ), derived from the luminosity and width of  $H\beta$ .

*Subject headings:* galaxies: active — galaxies: Seyfert – quasars: emission lines

## 1. Introduction

It is often assumed that the narrow emission lines in active galactic nuclei (AGN) are indicative of some approximately stable, quiescent pool of gas that is being excited or illuminated by the central source. Emission lines that originate in the narrow line region (NLR) are commonly used to obtain the systemic redshift (De Robertis 1985; Marziani et al. 1996; Richards et al. 2002) or as a proxy for the stellar velocity dispersion (Shields et al. 2003). Most often it is the [O III]  $\lambda 5007$  line that is used, as it is usually the strongest and cleanest narrow line in the optical region of the spectrum.

The validity of the assumptions that the  $\lambda 5007$  line is a good indicator of systemic redshift or stellar velocity dispersion rests primarily on extrapolation of studies of low luminosity objects, such as those by Heckman et al. (1981), Vrtilek (1985), Nelson and Whittle

(1996), and Nelson (2000). However, even these studies of the NLR characteristics in lower luminosity Seyfert galaxies suggest systematic departures from symmetry and stability are not uncommon. Heckman et al. (1981) and subsequent studies found (1) that the  $\lambda 5007$  line tends to be asymmetric, with a sharper falloff to the red than to the blue, and (2) that the redshift of the  $\lambda 5007$  line tends to be negative compared with the systemic velocity derived from the stellar absorption lines.

Several recent studies have explored some of the characteristics of the [O III]  $\lambda 5007$  line in AGNs. Zamanov et al. (2002) studied a sample of about 200 low redshift AGN, most of which were luminous enough to be considered QSOs. Under the assumption that the redshift derived from the broad  $H\beta$  line is the systemic value, they found that the  $\lambda 5007$  line gave a consistent redshift 90% of the time, but that, among the outliers, blueshifts were three times as common as redshifts. They investigated seven objects with the largest blueshifts, and found that they fell preferentially among the objects at the strong Fe II - narrow  $H\beta$  end of the Eigenvector 1 sequence (Boroson and Green 1992). In order to overcome the limitation of the assumption that  $H\beta$  gives the systemic redshift, they noted that for one of their blue outliers, I Zwicky 1, other observations of the host galaxy give a redshift consistent with the  $H\beta$  line and not the [O III] line. A consistent finding comes from the Veron-Cetty, Veron, & Goncalves (2001) study of narrow line Seyfert 1 galaxies (NLS1s) in which it was found that approximately half of their sample had a broad, blueshifted [O III]  $\lambda 5007$  line in addition to the narrow component assumed to be at the systemic velocity.

Boroson (2003) and Nelson et al. (2004) studied the [O III]  $\lambda 5007$  line in order to explore the utility of the width of this line as a surrogate for the stellar velocity dispersion. The Boroson (2003) study looked at a sample of 107 QSOs from the Sloan Digital Sky Survey (SDSS) Early Data Release (EDR), while the Nelson et al. (2004) study used new spectra of approximately 60 low-redshift PG QSOs. The technique used in both studies was to plot the width of the  $\lambda 5007$  line against black hole mass derived using the  $H\beta$  broad line FWHM and the luminosity at  $\lambda 5100$  in the rest frame,  $L_{5100}$ . The tight correlation between black hole mass and stellar velocity dispersion (Tremaine et al. 2002) in normal galaxies was the reference for the expected relationship. Both studies found that the [O III] widths show some correlation with black hole mass, but the scatter is large. Nelson et al. (2004) found that the more asymmetric [O III] lines have widths that are closer to those predicted by the Tremaine et al. (2002) fit. That study also found a correlation between [O III] line asymmetry and Eigenvector 1, in that objects with greater asymmetry were more likely to be at the strong Fe II end of the sequence, presumably correlating with higher  $L/L_{Edd}$ .

The study reported here is an effort to explore in greater detail and more quantitatively the behavior of the [O III]  $\lambda 5007$  line, by analyzing a larger sample of objects in which the

systemic velocity can be unambiguously determined. By combining a number of measurements of this line with other observed and derived properties, a better understanding of the geometric and kinematic structure in which the [O III] emission arises may emerge. A cosmology with  $H_0 = 71 \text{ km s}^{-1} \text{ Mpc}^{-1}$ ,  $\Omega_M = 0.27$  and  $\Omega_\Lambda = 0.73$  is used throughout this paper.

## 2. The Sample

The sample of QSOs was drawn from Data Release 1 (DR1) (Abazajian et al. 2003) of the Sloan Digital Sky Survey. The parent sample, which numbered about 3300, included all spectroscopically observed objects identified as QSOs having a redshift less than 0.5. From this list, those with spectroscopic signal-to-noise less than 15 in the R band (SN\_R in the FITS header) were removed, leaving 804 objects. The redshift distribution and absolute magnitude distribution (in the I band) for the sample are shown in figure 1. The spectra were corrected to rest wavelengths, adopting the SDSS value of the redshift stored in the header of each object.

These 804 spectra were inspected individually in the regions around the [O II]  $\lambda 3727$  doublet, the [N II]  $\lambda 6584$  line, and the [S II]  $\lambda 6717$  and  $\lambda 6731$  lines. When visible, the wavelength of each of these lines was measured, by fitting a gaussian to the top half of the line. These wavelengths were then converted to redshifts, using the vacuum wavelengths  $3728.30\text{\AA}$ ,  $6585.27\text{\AA}$ ,  $6718.29\text{\AA}$ , and  $6732.67\text{\AA}$  as the rest values for the lines. At least one of these lines could be measured in 654 of the 804 objects and at least two of the lines from different ions could be measured in 399 of the objects.

Figure 2 shows the distributions of relative redshifts for each of the three ions. The histograms show the redshift of the identified line (or the average of the two [S II] lines) relative to the redshifts of any of the other lines that were measured. The average relative redshifts are 13.0, -11.2, and -3.6  $\text{km s}^{-1}$  for [O II], [N II], and [S II] respectively. The corresponding standard deviations of the distributions are 39, 32, and 25  $\text{km s}^{-1}$ . It is likely that the [N II] measurements are shifted a bit to the blue (negative velocities) because this narrow line typically lies on the red wing of the broad  $H\alpha$  line. Part of the apparent shift of the [O II] distribution to positive velocity may be due to the fact that, in most cases, its redshift is being calculated relative to the anomalously blue [N II] line. An additional factor which may also account for the greater width of the [O II] distribution is that this ‘line’ is actually a doublet with a separation between components of about  $2.7\text{\AA}$ . An average value for the centroid of the blended components is undoubtedly not a good guess in some cases.

Despite the slight differences in mean and width of the distributions, they are all roughly symmetric, and it is likely that these lines indicate the systemic velocity of the galaxy. All of these lines from singly ionized species have low critical densities, and so they arise either in the outer parts of the narrow line region (NLR) or even further out, in the interstellar medium of the host galaxy itself. The 3 arcsecond diameter of the SDSS fibers corresponds to a physical diameter of about 10.5 kpc at the sample median redshift of 0.22. The mean of all visible low ionization lines in each object was adopted as its systemic redshift, and the spectra were adjusted to reflect rest wavelengths using these new, small offsets.

From these corrected spectra, the wavelength of the [O III]  $\lambda 5007$  line was measured in each object in a manner similar to that in which the low ionization lines were measured. These [O III] wavelengths were converted to a relative velocity using a vacuum rest wavelength of 5008.24 Å for this line. Figure 3 shows the distribution of these [O III] redshifts relative to the systemic redshift calculated from the low ionization lines. The solid histogram represents all the objects for which a low ionization systemic redshift could be determined and the [O III]  $\lambda 5007$  wavelength could be measured (638 objects; the total [O III] sample). The dotted histogram represents only the objects for which low ionization redshifts could be determined from two or more ions (399 objects; the high confidence [O III] sample). The bottom panel of this figure shows the sum of the redshift distributions for the three low ionization lines, in each case relative to the one or two other lines measured.

The low ionization line distribution is well fit by a gaussian with a mean of zero (by construction) and a width ( $\sigma$ ) of 35 km s<sup>-1</sup>, a fraction of which is due to the slight shift between the distributions. The [O III] distribution, however, has a broad shoulder on the blueshifted side, with a sprinkling of objects out to -400 km s<sup>-1</sup>. Approximately half the objects might be considered to be in a distribution like that for the low ionization lines with the other half on the blueshifted side. For the total [O III] sample, 135 (21%) of the 638 values have positive (redshifted) relative velocities; this number is 93 (23%) of 399 values for the high confidence sample. Note that both the total [O III] sample and the high confidence [O III] sample are biased within the original sample of DR1 objects toward the low redshift and low luminosity end. This bias is due to the fact that the low ionization narrow lines are more commonly found in the lower luminosity objects. The dashed and dotted lines in the two panels of Figure 1 show the distributions for the total [O III] and high confidence [O III] samples respectively.

### 3. Properties of Objects with Different [O III] Redshifts

In order to compare the properties of AGN with different [O III] velocity shifts, four subsamples were constructed. The subsamples are composed of about a dozen objects from the high confidence sample with [O III] velocities from the most blueshifted extreme of the distribution (the VB sample), the moderately blueshifted region (the B sample), the region in which the [O III] velocities are in good agreement with the systemic redshift (the N sample), and the most redshifted extreme of the distribution (the R sample).

For each object in these subsamples, the Fe II emission was measured and subtracted using the template and the technique developed in Boroson and Green (1992). The continuum was then subtracted and the FWHM of the  $H\beta$  line and the FWHM and asymmetry index A20 (Whittle 1985) of the [O III]  $\lambda 5007$  line were measured. Table 1 lists the properties of each object in the subsamples, including the absolute magnitude in the I band (from the I ‘PSF’ magnitude listed in the SDSS DR1 database), the measured shift in the [O III]  $\lambda 5007$  line, the equivalent width of the Fe II multiplets between  $\lambda 4434$  and  $\lambda 4684$ , the FWHM of  $H\beta$  and [O III]  $\lambda 5007$ , and the A20 value and equivalent width of the [O III]  $\lambda 5007$  line. Also listed are values of  $\log M_{BH}$  and  $\log L/L_{Edd}$  computed from the FWHM  $H\beta$  and the luminosity at  $\lambda 5100$  in the rest frame, which was calculated from the R band PSF magnitude. The [O III] FWHM values are corrected for the instrumental resolution, about  $150 \text{ km s}^{-1}$ . At the bottom of the table, average values of each quantity, for each of the four subsets, are given.

Initially, an attempt was made to use the tabulated  $H\beta$  width values from the SDSS database. Comparison with the final measured values shows that they are not a reliable indicator of what is conventionally used as the FWHM of this line. Only about 50% of the database values are within 20% of the measured widths. The discrepancies arise from (1) the inclusion of the narrow component in the automatic measurement, (2) the departure of the profile from a Gaussian, and (3) effects due to contamination by other lines - particularly Fe II.

Aside from the [O III] velocity values that characterize each sample, the statistical difference among the samples are limited to a few properties. Among the B, N, and R samples, there are no significant differences in the distribution of properties measured. The VB sample is differentiated from the other three samples in having narrower  $H\beta$  lines and broader [O III]  $\lambda 5007$  lines. The narrower  $H\beta$  lines result in the VB sample having smaller black hole mass and larger  $L/L_{Edd}$  on average than any of the other samples. It is worth noting that the VB sample does not differ from the other samples in the distribution of [O III] line asymmetry, A20.

#### 4. Discussion

It was previously known that among the objects with blueshifted [O III], Narrow Line Seyfert 1s (NLS1s), which have  $H\beta$  FWHM values less than  $2000 \text{ km s}^{-1}$  and are thought to be high  $L/L_{Edd}$  objects, are overrepresented. Zamanov et al. (2002) studied a small sample of objects with extreme [O III] blueshifts, greater than  $250 \text{ km s}^{-1}$  relative to the peak of the  $H\beta$  line, drawn from a heterogeneous sample of 216 objects. These authors found that the seven extreme objects all had  $H\beta$  FWHM values below  $4000 \text{ km s}^{-1}$ , with three of the extreme objects falling in the NLS1 regime. About half of the sample from which these objects were drawn has  $H\beta$  FWHM values below  $4000 \text{ km s}^{-1}$ .

Both the derived black hole mass and the Eddington ratio ( $L/L_{Edd}$ ) depend on the  $H\beta$  FWHM and the luminosity. Limiting the comparison to just the VB and N subsamples, the average luminosities of the two are not significantly different but the  $H\beta$  widths are quite different -  $2175 \text{ km s}^{-1}$  for the VB sample vs  $4456 \text{ km s}^{-1}$  for the N sample. This leads to black hole masses substantially smaller and Eddington ratios substantially larger on average for the VB objects. A comparison of the distributions, however, shows that the difference in Eddington ratio is far more significant than that in black hole mass (0.8% vs 4.5% probability from a student t-test).

Table 1 also shows, however, that not all narrow  $H\beta$ , high Eddington ratio objects have large [O III] blueshifts and that not all the objects with large [O III] blueshifts have narrow  $H\beta$  and high Eddington ratios. In order to investigate whether other properties are related to the distinction between VB and non-VB objects, another subsample, consisting of 12 objects that appeared to be NLS1s with [O III] velocities near zero, was defined. The same  $H\beta$  and [O III] characteristics were measured for this sample, called the N-NLS1 sample, and these values are also given in Table 1. Other than [O III] velocity, this N-NLS1 subsample has properties indistinguishable from the VB sample, except for the width of the [O III] line, which has an average of  $335 \text{ km s}^{-1}$ , consistent with the N value of  $328 \text{ km s}^{-1}$ , and inconsistent with the VB value of  $523 \text{ km s}^{-1}$ . This is in contrast to the smaller average black hole masses calculated for the VB (and N-NLS1) objects, and therefore in conflict with the idea that the [O III] width is indicative of the stellar velocity dispersion, which is, in turn, correlated with the black hole mass. Thus, one could characterize the situation with two statements: (1) objects with higher Eddington ratio are more likely to have large [O III] blueshifts; and (2) objects with large [O III] blueshifts have anomalously broad [O III] emission lines.

This result is shown graphically in Figure 4, in which black hole mass is plotted against the log of the [O III] line width ( $\sigma$ ) for the separate subsamples. Each subsample is plotted as a different symbol, and the mean values for each subsample are plotted as large symbols

of the same type. The line in Figure 4 is the Tremaine et al. (2002) relation between black hole mass and stellar velocity dispersion. It is apparent that the VB subsample (solid circles) have similar black hole masses to the N-NLS1 subsample (open circles), but that the [O III] widths are much larger for the VB objects, which lie substantially below or to the right of the line. It is interesting that the N-NLS1 subsample also lies slightly below or to the right of the line, suggesting the possibility of a similar, though smaller discrepancy between stellar velocity dispersion and [O III] line width.

It has been claimed that objects with large [O III] blueshifts also are more likely to show blue asymmetries in that line. That does not appear to be the case in this sample. There is no statistically significant difference in the distribution of A20 values between any of the subsamples. Only six of the 59 A20 values do not show a blue asymmetry, and, of these, two indicate no asymmetry in either direction. It appears that blue asymmetries are equally dominant in objects of all types, both with and without [O III] blueshifts.

The distribution of equivalent width of the [O III]  $\lambda 5007$  line among subsamples is also worth noting. While there is no formal difference between the distributions within, admittedly small, subsamples, five of the 12 objects in the N sample have equivalent widths larger than the largest object in the VB sample. Thus, the N sample is characterized by a much broader distribution (standard deviation = 31 Å) of  $\lambda 5007$  equivalent widths than is the VB sample (standard deviation = 6 Å). The distributions differ formally at the 90% significance level.

Many previous studies have speculated on the cause of [O III] emission with an extended blue wing, a broad underlying blueshifted component, or a blueshifted line center. The explanations include both outflow models and inflow models. Outflow models are motivated by the idea that objects such as NLS1s have characteristics that would support radiation pressure as a mechanism for accelerating such flows. Imaging observations (Ruiz et al. 2005), which show the [O III] emission coming from a biconical region in many cases, support this idea. These models must posit some obscuring screen, depending on the assumed scale of the outflow, that blocks the observers view of the material on the far side. This could be the ‘dusty torus’ or it could be a larger, central plane of interstellar material in the host galaxy. Inflow models have the advantage that they produce the line asymmetry by mixing the obscuring material with the NLR clouds, thus, no additional structure that happens to match the size of the outflowing, emitting material is needed. It is the material on the near side that is invisible, since the backsides of these clouds are being illuminated. These models are supported by the idea that the emitting clouds in NLS1s are the most dense - as deduced from studies of lines arising from ions such as Fe II, Ca II, and Na I (Ferland and Persson 1989). Thus, both of these types of models are consistent with the increasing frequency of

[O III] blueshifts with increasing  $L/L_{Edd}$ .

Although the new findings (as well as previous investigations) do not clearly distinguish between the two models, a number of interesting conclusions may be drawn. Radial motion of narrow line emitting clouds is present in almost all objects. This is the only way to account for the common occurrence of line peak blueshifts and the ubiquitous presence of the line asymmetry. In the inflow model, we never see the near side of the clouds on the near side of the nucleus; in the outflow model, we never see the clouds on the far side of the nucleus. This latter point is interesting because it implies that the scale of narrow line emission is not large relative to some obscuring plane in the center of the active galaxy, whether that is a structure related to the accretion flow or it is the central plane of the galaxy. This also suggests that the [O III] width is not generally a suitable surrogate for the stellar velocity dispersion, but rather, represents the radial velocity gradient in the outflow or inflow.

Why have previous studies found the [O III] line width to be correlated with stellar velocity dispersion? One possible explanation is that the outflow (or inflow) of the narrow-line emitting material is affected by the black hole mass, either through gravity or through radiation pressure. If the [O III] line width is indicative of the maximum radial velocity, then it would be correlated with the black hole mass. At the same time, the stellar velocity dispersion is correlated with the black hole mass, and the two widths appear to be correlated with each other.

The most apparent flaw in this picture comes from the objects with extreme [O III] blueshifts. These are predominantly objects with small black hole masses and yet they have very broad [O III] lines. Furthermore, they are, in all other ways, identical to another group of objects, the N-NLS1 subsample. Clearly another parameter is required. One possibility for this parameter is orientation; objects with larger blueshifts and broader lines are those in which the outflow is directed closer to the line of sight.

Putting these pieces together yields the following picture: At a given  $L/L_{Edd}$ , outflow (or inflow) velocity is larger in objects with larger black hole mass. At a given black hole mass, outflow velocity is larger in objects with larger  $L/L_{Edd}$ . In addition, as one goes to larger  $L/L_{Edd}$ , the cone angle of the outflow decreases, and in the objects with large  $L/L_{Edd}$ , one sees a range from small outflow velocities (in objects in which the axis of the outflow is in the plane of the sky) to large outflow velocities (in which the axis is along the line of sight). Whether this picture extends all the way to truly edge-on objects in which one sees both sides of the outflow, and consequently symmetric lines with twice the flux, is not clear given the small number of objects studied here. This model implies that the other parameters that distinguish objects -  $H\beta$  width, Fe II strength, [O III] equivalent width - are not primarily orientation dependent.



An interesting comparison can be made with the velocity distribution of the peak of the C IV line, studied in higher redshift SDSS quasars by Richards et al. (2002). Working with composite spectra generated from large samples of objects divided by C IV blueshift relative to the Mg II line, these authors found that more blueshifted C IV lines occurred as a result of the red wing of the line being obscured. They suggested that this obscuration is due to a central screen of finite geometrical thickness, which is optically thin seen face-on but becomes thicker with increasing angle. Note that this is, in some sense, opposite to the scheme proposed here, in which the objects with the largest blueshifts are those seen closest to face-on. In any case, the geometry and kinematics of the C IV-emitting clouds and the [O III]-emitting clouds may be different, and so the explanations may not be inconsistent.

## 5. Conclusions

Characteristics of AGNs with blueshifted [O III] lines have been reported previously. However, conclusions have been based on small samples, with heterogeneous data, or requiring dubious assumptions. In this study, a large, uniform sample of AGNs from the SDSS DR1 have been analyzed. Objects with discrepant [O III] redshifts have been identified and subsamples constructed to explore the properties of objects populating different regions in the [O III] relative velocity distribution. Analysis of these samples yields the following conclusions.

- 1) A significant fraction, as many as half, of all AGNs show [O III] emission that is blueshifted to the point that the line peak is shifted by tens to hundreds of  $\text{km s}^{-1}$ .
- 2) This shift is a true shift relative to the systemic velocity, as determined from the low ionization narrow forbidden lines.
- 3) The AGNs with the largest blueshifted [O III] lines tend to have high  $L/L_{\text{Edd}}$ , using black hole masses determined from their luminosities and  $H\beta$  widths. However, this is not a tight correlation; there are high  $L/L_{\text{Edd}}$  objects that do not show blueshifts, and lower  $L/L_{\text{Edd}}$  objects that do.
- 4) The single anomalous property common to all the objects with highly blueshifted [O III] emission is the large width of the [O III] lines. These average more than 50% broader than those in similar objects that have [O III] close to the systemic velocity.
- 5) Conversely, the blueshifted [O III] lines do not tend to be any more asymmetric or any weaker in strength than the non-blueshifted ones. All the subsamples show a similar tendency to have a sharp red edge to the line and a blue edge that is shallow, or has a wing

or a shoulder.

While these characteristics do not identify a unique model, simple arguments suggest that the maximum radial velocity of the [O III] emitting clouds is controlled by both black hole mass and Eddington ratio. A radial velocity gradient is primarily responsible for the line width, which then allows an orientation parameter to play a role. The apparent correlation of [O III] line width with stellar velocity dispersion in previous studies may be due to the fact that both of these widths are somewhat dependent on black hole mass.

I thank G. Richards, P. Hall, J. Shields, G. Shields, and A. Laor for helpful discussions. Funding for the creation and distribution of the SDSS Archive has been provided by the Alfred P. Sloan Foundation, the Participating Institutions, the National Aeronautics and Space Administration, the National Science Foundation, the Department of Energy, the Japanese Monbukagakusho, and the Max Planck Society. The SDSS Web site is <http://www.sdss.org>. The Participating Institutions in the SDSS are the University of Chicago, Fermilab, the Institute for Advanced Study, the Japan Participation Group, the Johns Hopkins University, the Max Planck Institute for Astronomy, the Max Planck Institute for Astrophysics, New Mexico State University, Princeton University, the United States Naval Observatory, and the University of Washington.

## REFERENCES

- Abazajian, K. et al. 2003, *AJ*, 126, 2081
- Boroson, T. A. 2003, *ApJ*, 585, 647
- Boroson, T. A. & Green, R. F. 1992, *ApJS*, 80, 109
- De Robertis, M. 1985, *ApJ*, 289, 67
- Ferland, G. J. & Persson, S. E. 1989, *ApJ*, 347, 656
- Heckman, T. M., Miley, G. K., van Breugel, W. J. M., & Butcher, H. R. 1981, *ApJ*, 247, 403
- Marziani, P., Sulentic, J. W., Dultzin-Hacyan, D., Calvani, M., & Moles, M. 1996, *ApJS*, 104, 37
- Nelson, C. H. 2000, *ApJ*, 544, 91
- Nelson, C. H. & Whittle, M. 1996, *ApJ*, 465, 96

- Nelson, C. H., Plasek, A., Thompson, A., Gelderman, R., & Monroe, T. 2004, AGN Physics with the Sloan Digital Sky Survey, G. Richards and P. Hall, ASP Conference Series, 311, 83
- Richards, G.T., Vanden Berk, D.E., Reichard, T. A., Hall, P. B., Schneider, D. P., SubbaRao, M., Thakar, A.R., & York, D. G. 2002, AJ, 124, 1
- Ruiz, J. R., Crehshaw, D. M., Kraemer, S. B., Bower, G. A., Gull, T. R., Hutchings, J. B., Kaiser, M. E., and Weistrop, D. 2005, AJ, 129 73
- Shields, G. A., Gebhardt, K., Salviander, S., Wills, B. J., Xie, B., Brotherton, M. S., Yuan, J., & Dietrich, M. 2003, ApJ, 583, 124
- Tremaine, S., et al. 2002, ApJ, 574, 740
- Veron-Cetty, M.-P., Joly, M., & Veron, P. 2004, A&A, 417, 515
- Vron-Cetty, M.-P., Vron, P., & Gonalves, A. C. 2001, A&A, 372, 730
- Vrtilek, J. M. 1985, ApJ, 294, 121
- Whittle, M. 1984, MNRAS, 213, 1
- Zamanov, R., Marziani, P., Sulentic, J. W., Calvani, M., Dultzin-Hacyan, D., & Bachev, R. 2002, ApJ, 576, 9

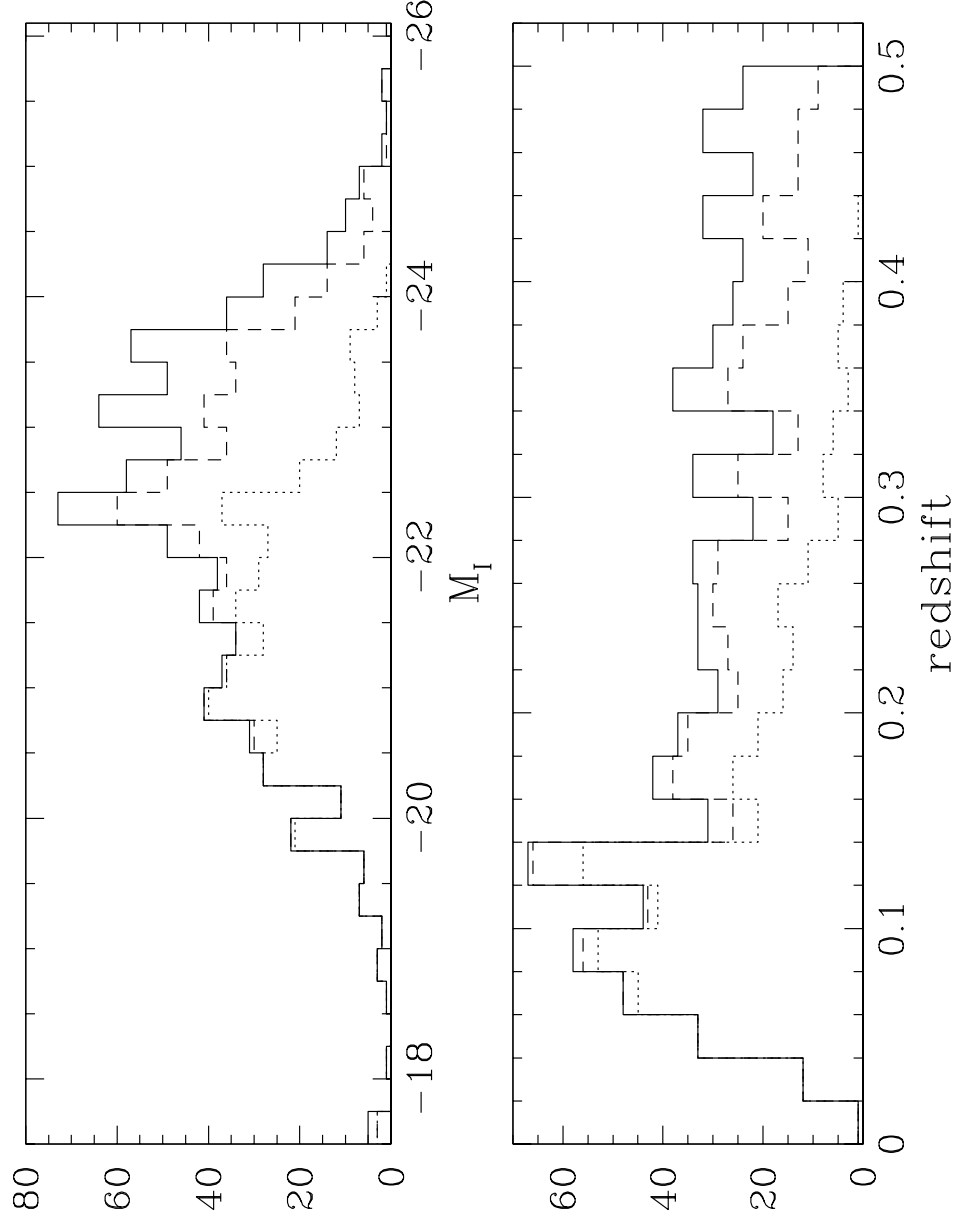


Fig. 1.— Distribution of absolute magnitude in the I band (top) and redshift (bottom) for the sample of 804 SDSS DR1 quasars studied. The dashed line indicates those for which any low ionization lines were measured. The dotted line indicates those for which lines from two or more low ionization species were measured.

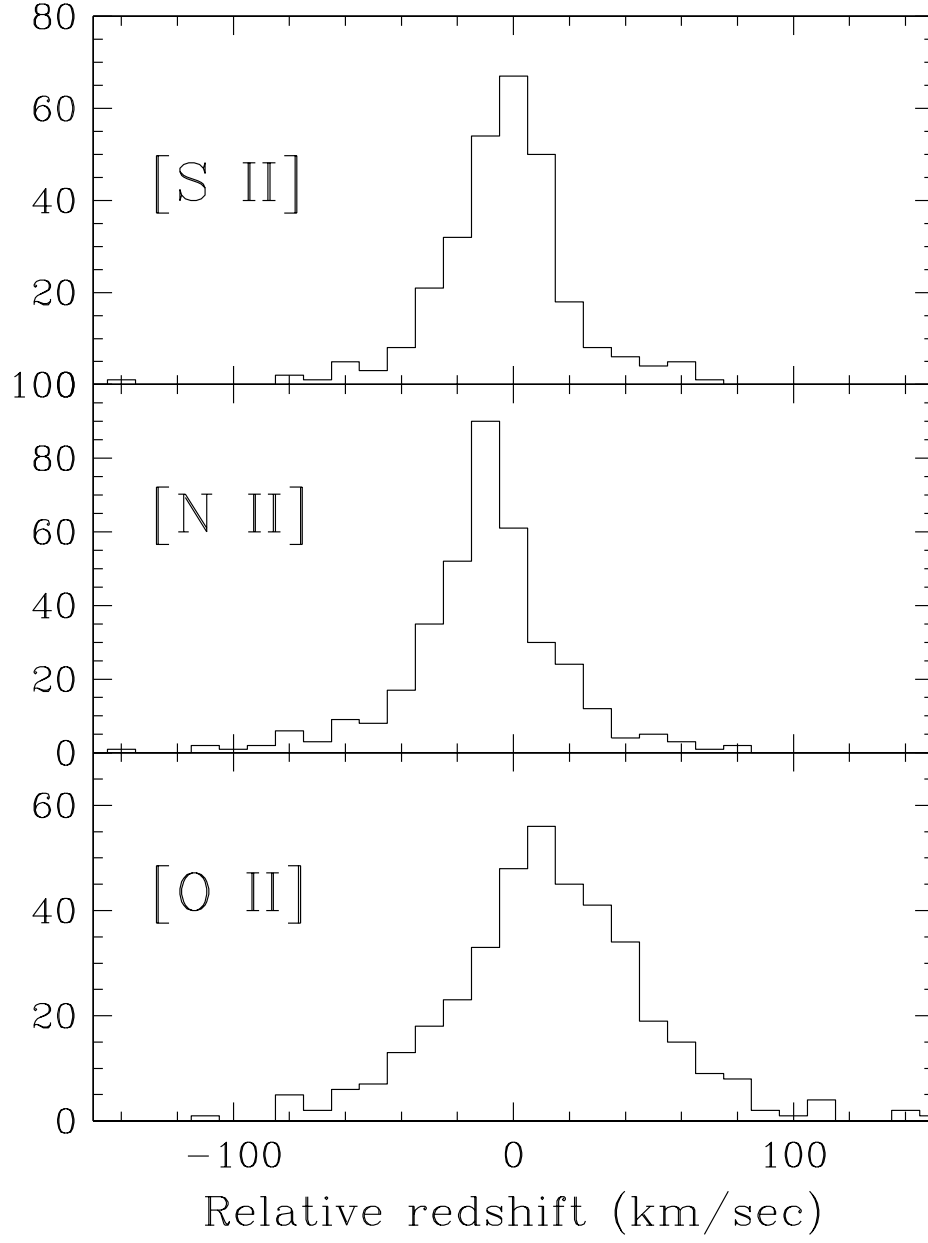


Fig. 2.— For each of the three ions indicated, the distribution of redshift relative to that of other low ionization lines.

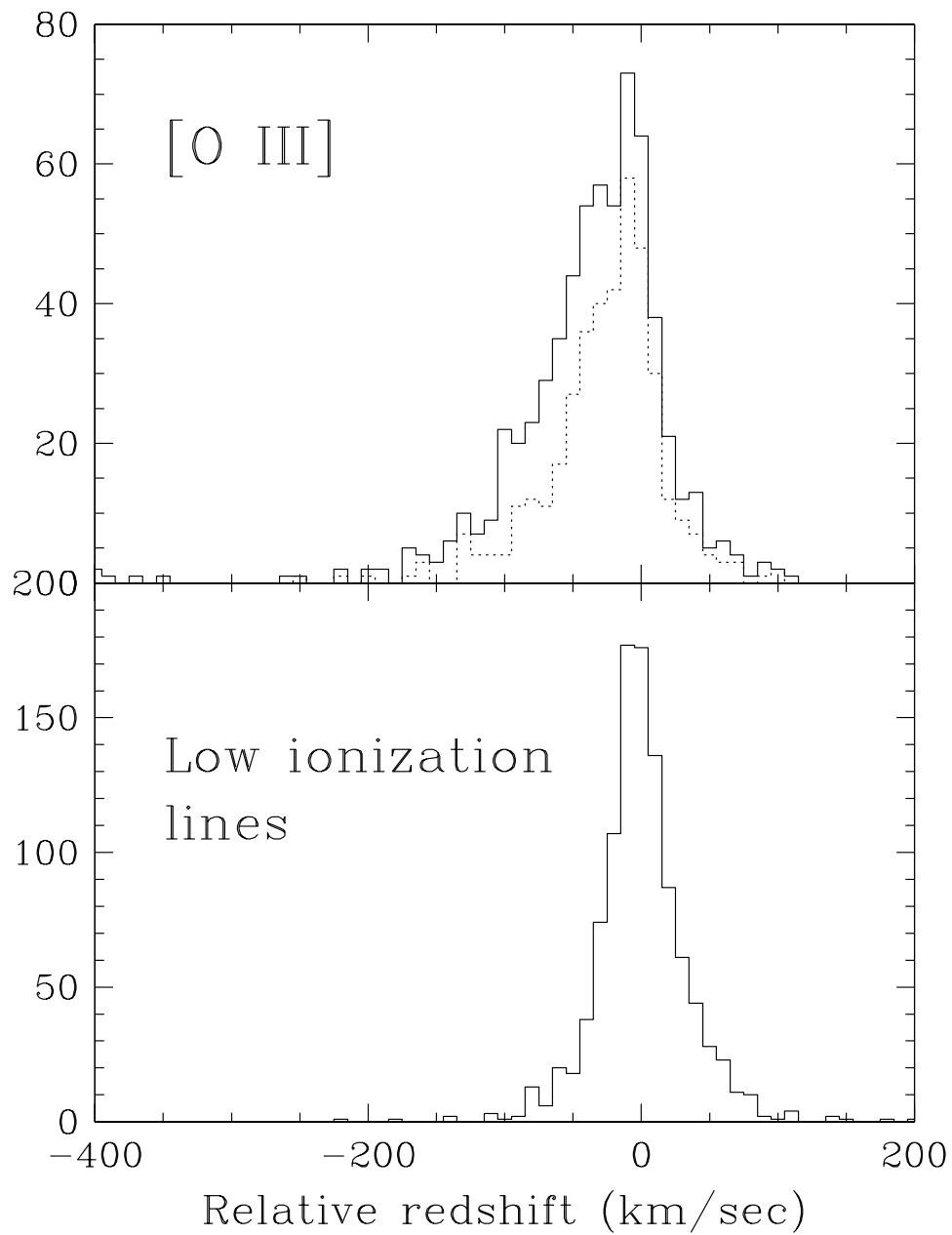


Fig. 3.— Relative redshift distributions for all measurements of low ionization lines (bottom) and for the [O III]  $\lambda 5007$  line (top). The dotted line in the top panel shows the objects for which two or more low ionization species are used to calculate the systemic velocity.

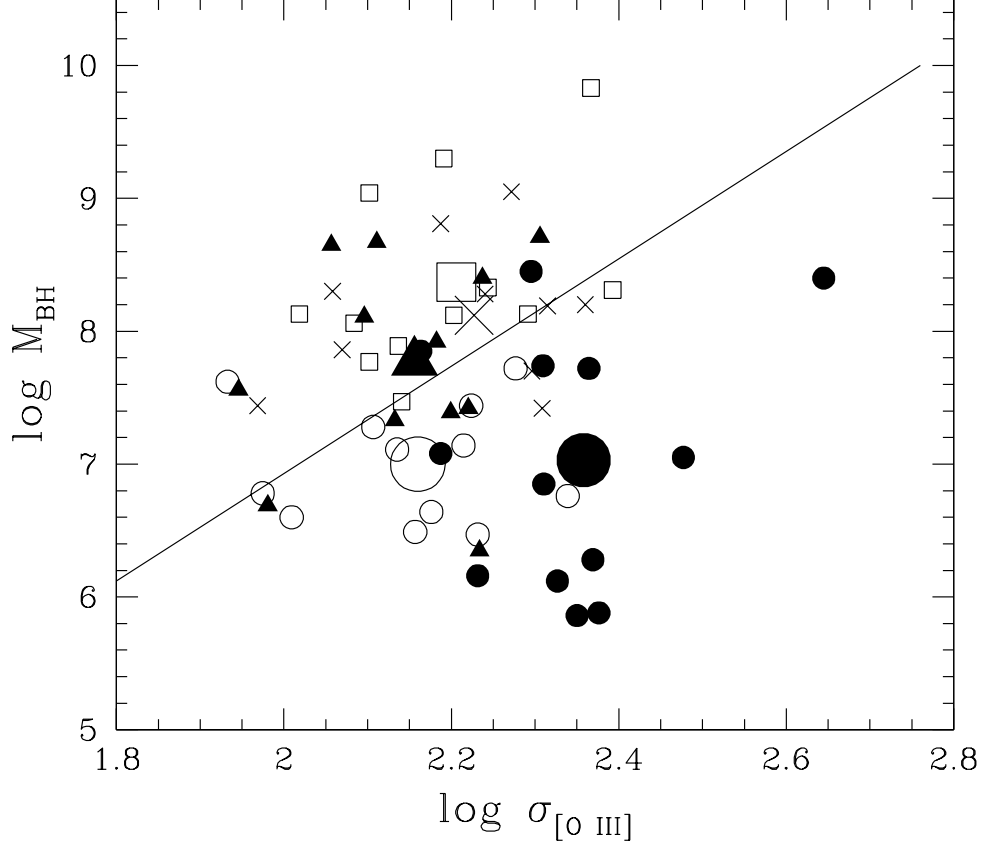


Fig. 4.— Black hole mass plotted against the [O III] line width. The VB subsample is plotted as solid circles, the B subsample is plotted as open squares, the N subsample is plotted as solid triangles, the R subsample is plotted as crosses, and the N-NLS1 subsample is plotted as open circles. The large symbols of each type show the position of the mean values for that subsample. The line is the Tremaine et al. (2002) fit to the relation between black hole mass and stellar velocity dispersion.

Table 1. Properties of 5 AGN Subsamples

| subsample | SDSS J             | z      | $M_I$  | $v_{[OIII]}$ | EW Fe II | FWHM H $\beta$ | log $M_{BH}$ | log $L/L_{Edd}$ | FWHM [O III] | A20 [O III] | EW [O III] |
|-----------|--------------------|--------|--------|--------------|----------|----------------|--------------|-----------------|--------------|-------------|------------|
| VB        | 013521.68−004402.2 | 0.0985 | −20.91 | −252.8       | 32       | 1994           | 7.05         | 0.32            | 690          | 0.248       | 20.1       |
| VB        | 011929.06−000839.7 | 0.0900 | −20.74 | −218.6       | 38       | 715            | 6.12         | 1.19            | 488          | 0.220       | 15.5       |
| VB        | 150521.92+014149.9 | 0.1580 | −21.31 | −165.9       | 54       | 649            | 6.28         | 1.38            | 538          | 0.052       | 24.7       |
| VB        | 154259.49+030653.3 | 0.0655 | −19.77 | −162.3       | 17       | 712            | 5.86         | 1.09            | 515          | 0.268       | 15.5       |
| VB        | 124635.25+022208.8 | 0.0482 | −20.44 | −159.3       | 43       | 751            | 6.16         | 1.15            | 392          | 0.208       | 18.6       |
| VB        | 032606.75+022539.9 | 0.1273 | −21.10 | −158.1       | 58       | 508            | 5.88         | 1.51            | 547          | 0.214       | 12.0       |
| VB        | 104153.60+031500.7 | 0.0934 | −20.45 | −133.6       | 41       | 2433           | 7.08         | 0.08            | 354          | 0.041       | 20.4       |
| VB        | 131843.87+004732.2 | 0.3930 | −23.04 | −131.8       | 104      | 4232           | 8.45         | −0.02           | 454          | 0.438       | 16.6       |
| VB        | 171829.01+573422.4 | 0.1008 | −21.16 | −130.6       | 50       | 1452           | 6.85         | 0.63            | 470          | 0.229       | 12.4       |
| VB        | 082405.19+445246.1 | 0.2196 | −22.41 | −126.4       | 32       | 2439           | 7.72         | 0.36            | 532          | 0.231       | 5.1        |
| VB        | 132135.33−001305.8 | 0.0822 | −21.17 | −118.6       | 21       | 4498           | 7.85         | −0.35           | 335          | 0.051       | 27.5       |
| VB        | 171049.90+652102.1 | 0.3857 | −23.52 | −116.8       | 73       | 5351           | 8.40         | −0.33           | 1015         | 0.228       | 13.2       |
| VB        | 091459.58+023510.9 | 0.2329 | −22.35 | −116.2       | 21       | 2543           | 7.74         | 0.31            | 469          | 0.242       | 11.2       |
| B         | 113626.06+021144.2 | 0.1374 | −21.22 | −55.1        | 35       | 2870           | 7.47         | 0.05            | 318          | 0.133       | 10.9       |
| B         | 021218.32−073719.7 | 0.1738 | −22.45 | −54.1        | 74       | 2446           | 8.12         | 0.52            | 367          | 0.126       | 15.1       |
| B         | 022417.17−092549.3 | 0.3115 | −22.82 | −53.9        | 41       | 8479           | 9.04         | −0.63           | 291          | 0.195       | 31.7       |
| B         | 162650.24−001731.8 | 0.2685 | −21.68 | −53.3        | 54       | 5871           | 8.31         | −0.48           | 568          | 0.148       | 19.4       |
| B         | 012946.72+150457.3 | 0.3652 | −23.57 | −53.3        | 0        | 9346           | 9.30         | −0.63           | 357          | 0.000       | 32.4       |
| B         | 080644.41+484149.3 | 0.3701 | −23.68 | −52.1        | 0        | 16868          | 9.83         | −1.14           | 535          | 0.495       | 29.5       |
| B         | 101911.34+015354.7 | 0.1886 | −22.21 | −52.1        | 36       | 5699           | 8.33         | −0.44           | 403          | 0.000       | 49.5       |
| B         | 074948.26+345444.0 | 0.1318 | −22.28 | −52.1        | 71       | 2920           | 7.77         | 0.15            | 291          | 0.294       | 9.0        |
| B         | 085635.86+521729.6 | 0.1443 | −21.15 | −51.5        | 25       | 6279           | 8.13         | −0.64           | 240          | 0.442       | 12.4       |
| B         | 154751.94+025550.9 | 0.0980 | −21.47 | −51.5        | 35       | 5868           | 8.13         | −0.56           | 450          | 0.285       | 27.2       |
| B         | 172033.62+580829.6 | 0.1597 | −21.91 | −50.9        | 14       | 4353           | 8.06         | −0.22           | 279          | 0.136       | 24.5       |
| B         | 142245.79+630739.2 | 0.1608 | −22.20 | −50.9        | 71       | 3194           | 7.89         | 0.09            | 315          | 0.125       | 10.6       |
| N         | 083202.16+461425.7 | 0.0459 | −19.88 | −1.8         | 23       | 1773           | 6.69         | 0.31            | 220          | −0.040      | 8.5        |
| N         | 130002.92−010601.8 | 0.3074 | −22.72 | −1.2         | 0        | 5575           | 8.65         | −0.27           | 262          | 0.105       | 63.7       |
| N         | 013527.85−004448.0 | 0.0804 | −20.62 | −1.2         | 21       | 3524           | 7.42         | −0.23           | 382          | 0.126       | 2.9        |
| N         | 035301.02−062326.4 | 0.0760 | −20.62 | −1.2         | 14       | 7190           | 8.11         | −0.82           | 287          | 0.159       | 7.7        |
| N         | 134952.84+020445.1 | 0.0328 | −19.99 | −1.2         | 0        | 3525           | 7.33         | −0.27           | 312          | 0.121       | 91.4       |
| N         | 150756.89+032037.3 | 0.1369 | −21.85 | −1.2         | 14       | 2204           | 7.39         | 0.34            | 364          | 0.245       | 44.0       |
| N         | 090821.74+522103.0 | 0.0759 | −20.27 | −0.6         | 22       | 1089           | 6.35         | 0.77            | 394          | 0.233       | 8.3        |
| N         | 113633.09+020747.5 | 0.2390 | −22.65 | 0.6          | 31       | 7456           | 8.71         | −0.61           | 465          | 0.329       | 9.6        |
| N         | 134617.54+622045.5 | 0.1165 | −22.28 | 0.6          | 40       | 8437           | 8.67         | −0.78           | 297          | 0.083       | 47.7       |
| N         | 170845.58+595716.2 | 0.2736 | −21.62 | 0.7          | 0        | 6254           | 8.40         | −0.52           | 397          | −0.077      | 72.6       |
| N         | 123440.96+675213.8 | 0.2740 | −22.41 | 1.8          | 68       | 1833           | 7.56         | 0.64            | 203          | −0.347      | 3.1        |
| N         | 154606.97+034757.0 | 0.1274 | −21.61 | 1.8          | 89       | 4612           | 7.92         | −0.35           | 350          | 0.463       | 17.9       |
| R         | 143847.54−000805.4 | 0.1040 | −20.83 | 33.5         | 51       | 5493           | 7.86         | −0.59           | 270          | 0.229       | 10.5       |
| R         | 003659.78+010544.4 | 0.1211 | −21.01 | 33.5         | 53       | 3053           | 7.44         | −0.04           | 214          | 0.132       | 7.9        |
| R         | 110057.71−005304.5 | 0.3777 | −23.78 | 38.9         | 70       | 6399           | 9.05         | −0.27           | 430          | 0.315       | 13.6       |
| R         | 030639.57+000343.2 | 0.1071 | −21.58 | 46.1         | 12       | 2585           | 7.42         | 0.15            | 468          | 0.175       | 37.5       |
| R         | 080322.48+433307.1 | 0.2761 | −22.32 | 52.7         | 14       | 4740           | 8.30         | −0.22           | 263          | 0.122       | 8.4        |
| R         | 141556.85+052029.6 | 0.1263 | −22.01 | 52.7         | 26       | 5313           | 8.20         | −0.41           | 527          | 0.182       | 59.4       |
| R         | 030144.20+011530.9 | 0.0747 | −20.89 | 65.3         | 28       | 4187           | 7.70         | −0.32           | 455          | 0.323       | 22.5       |
| R         | 163631.29+420242.5 | 0.0610 | −20.54 | 68.9         | 26       | 8131           | 8.19         | −0.94           | 475          | 0.238       | 6.4        |
| R         | 003847.97+003457.4 | 0.0805 | −20.93 | 71.9         | 41       | 8510           | 8.28         | −0.95           | 400          | 0.119       | 21.9       |
| R         | 015629.06+000724.4 | 0.3604 | −22.49 | 104.8        | 28       | 7350           | 8.81         | −0.55           | 354          | 0.257       | 16.5       |
| N-NLS1    | 081231.44+441620.8 | 0.2969 | −22.68 | −10.8        | 15       | 2058           | 7.72         | 0.56            | 435          | 0.269       | 25.7       |
| N-NLS1    | 035107.60−052637.1 | 0.0691 | −20.72 | −11.4        | 59       | 1356           | 6.76         | 0.67            | 502          | 0.213       | 12.2       |
| N-NLS1    | 123440.96+675213.8 | 0.2740 | −22.41 | 1.8          | 68       | 1833           | 7.62         | 0.67            | 197          | −0.315      | 3.0        |
| N-NLS1    | 075333.82+385722.2 | 0.1468 | −21.29 | −2.4         | 14       | 1807           | 7.14         | 0.48            | 377          | 0.013       | 21.0       |



Table 1—Continued

| subsample          | SDSS J             | z      | $M_I$  | $v_{[OIII]}$ | EW Fe II | FWHM H $\beta$ | log $M_{BH}$ | log $L/L_{Edd}$ | FWHM [O III] | A20 [O III] | EW [O III] |
|--------------------|--------------------|--------|--------|--------------|----------|----------------|--------------|-----------------|--------------|-------------|------------|
| N-NLS1             | 083202.16+461425.7 | 0.0459 | −19.88 | −1.8         | 13       | 1675           | 6.78         | 0.42            | 217          | 0.000       | 8.0        |
| N-NLS1             | 151956.57+001614.6 | 0.1144 | −21.32 | 4.2          | 45       | 1782           | 7.11         | 0.48            | 314          | 0.158       | 15.1       |
| N-NLS1             | 125227.32+032353.6 | 0.1328 | −21.65 | 15.6         | 26       | 1822           | 7.28         | 0.53            | 294          | 0.473       | 34.4       |
| N-NLS1             | 130713.25−003601.6 | 0.1700 | −22.49 | 5.0          | 35       | 1931           | 7.44         | 0.53            | 385          | 0.183       | 69.8       |
| N-NLS1             | 090821.74+522103.0 | 0.0759 | −20.27 | −0.6         | 22       | 1089           | 6.47         | 0.82            | 392          | 0.244       | 7.7        |
| N-NLS1             | 111407.35−000031.0 | 0.0727 | −19.90 | 7.2          | 11       | 1230           | 6.60         | 0.72            | 235          | 0.020       | 15.8       |
| N-NLS1             | 135444.34+024039.2 | 0.1385 | −20.86 | 4.8          | 46       | 936            | 6.49         | 1.02            | 330          | 0.327       | 59.8       |
| N-NLS1             | 131008.01+634103.6 | 0.1926 | −22.35 | 10.2         | 55       | 758            | 6.64         | 1.34            | 345          | 0.200       | 7.0        |
| Subsample Averages |                    |        |        |              |          |                |              |                 |              |             |            |
| VB                 | Sample Average     | 0.1612 | −21.41 | −153.2       | 45       | 2175           | 7.03         | 0.56            | 523          | 0.205       | 16.4       |
| B                  | Sample Average     | 0.2091 | −22.22 | −52.6        | 38       | 6183           | 8.37         | −0.33           | 368          | 0.198       | 22.7       |
| N                  | Sample Average     | 0.1488 | −21.38 | −0.2         | 27       | 4456           | 7.77         | −0.15           | 328          | 0.117       | 31.5       |
| R                  | Sample Average     | 0.1689 | −21.64 | 56.8         | 35       | 5576           | 8.12         | −0.41           | 386          | 0.209       | 20.5       |
| N-NLS1             | Sample Average     | 0.1441 | −21.32 | 1.8          | 34       | 1523           | 7.00         | 0.69            | 335          | 0.149       | 23.3       |